Building and Environment 193 (2021) 107651

Contents lists available at ScienceDirect

Building and Environment

journal homepage: http://www.elsevier.com/locate/buildenv

Study on mitigation of automobile exhaust pollution in an urban street canyon: Emission reduction and air cleaning street lamps

Ming-Hua Huang [a], Yu Huang [b], Jun-Ji Cao [b], Wen-Quan Tao [a,*]

[a] Key Laboratory of Thermo-Fluid Science and Engineering of MOE, Xi'an Jiaotong University, Xi'an, 710049, China
[b] Key Laboratory of Aerosol, SKLLQG, Institute of Earth Environment, Chinese Academy of Sciences, Xi'an, 710061, China

ARTICLE INFO

Keywords:
Street canyon
Emission reduction
Air cleaning street lamp
CFD

ABSTRACT

Affected by the rapid growth of the number of fuel motor vehicles, the automobile exhaust pollution in the street canyon is becoming more and more serious. Different from the pollution source control technology usually used for outdoor air pollution control, an air cleaning street lamp is designed in this work. A 3D steady numerical model with line source pollution is established to simulate the air flow and pollutant diffusion in street canyons and validated. Then, the distributions of pollutants in 90 scenarios of street canyons are numerically simulated. The results show that wind direction and wind speed have great influence on pollutants diffusion in street canyons. Air quality in street breathing zones is improved with the reduction of emission; however, the air quality inside the street canyon is still worse than that outside the street canyon. Scenario with air cleaning street lamps with four 45° downward air outlets is shown to work better in improving air quality. In most of the studied cases, air cleaning street lamps are found to be more effective than reducing emissions from automobiles. A better method to improve the air quality in street canyons is to combine emission reduction measures and air cleaning street lamps. For the high-pollution breathing zone under perpendicular, oblique and parallel approaching wind directions, by this better method the mean PM concentration decreases by 14.38%, 7.68% and 17.78%, respectively; the mean NO_x concentration decreases by 24.92%, 21.33% and 29.03%, respectively; the mean CO concentration decreases by 12.77%, 7.45% and 15.05%, respectively.

1. Introduction

With the development of economy and urbanization, the number of fuel vehicles increases rapidly. Increasing fuel vehicles has led to high traffic emissions, including nitrogen oxides (NO_x), carbon monoxide (CO), carbon dioxide (CO_2), volatile organic compounds (VOCs), hydrocarbons (HCs), and particulate matter (PM), which degrade ambient air quality and harm public health. High pollution levels are often observed in urban street canyons due to high traffic emissions and limited natural ventilation in streets flanked by buildings. Exposure to traffic-polluted air increases the risk of many human diseases, including respiratory disease, cardiovascular disease, diabetes, lung cancer, and so on [1–4]. A famous experiment, Harvard Six-City Study, which began in 1973 and lasted 16 years, showed a correlation between air pollution and mortality. In 2006, a study of extended follow-up to the Harvard Six-City Study [5] showed that cities with significant reductions in fine particulate matter in the air had significant reductions in mortality. For every 1 mg·m^{-3} drop in $PM_{2.5}$, the death rate falls by 3%, saving 75,000 deaths a year in the United States. So, improving the air quality of urban street canyons is very important, which is closely linked with the people's life and health.

Despite that microscale urban climate is primarily driven by mesoscale forcing, the flow inside an urban canyon, particularly the skimming flow, is essentially devoid of direct perturbations from mesoscale forcing. Under this circumstance, for the study at the street scale, computational fluid dynamics (CFD) technique is the common method [6,7]. It typically produces reasonable qualitative results, allows for more complex geometrical arrangements and is more flexible than laboratory or field experiments [8]. Previous studies have shown that the wind flow and pollutant dispersion patterns inside the urban canyon are mainly determined by the canyon geometry (in particular, the aspect ratio of the building height H to the street width W), wind direction and wind speed [9–11]. It is worthwhile to mention that street trees, the most common components of the urban environment, also determine pollutant dispersion and flow patterns [12,13]. It is found that [14] at a greater H/W (>0.7) pollutants inside the street canyon could not be

* Corresponding author.
E-mail address: wqtao@mail.xjtu.edu.cn (W.-Q. Tao).

https://doi.org/10.1016/j.buildenv.2021.107651
Received 3 December 2020; Received in revised form 13 January 2021; Accepted 24 January 2021
Available online 6 February 2021

ventilated easily; that perpendicular approaching wind direction is considered as the worst situation for pollutants to dilute from street canyons; and that high wind speed is conducive to the dilution of pollutants.

There are two general approaches for improving air quality: pollution source control and pollution transmission control. Pollution source control is an essential way to directly reduce the pollution intensity. To control the pollution source many regions of the world have issued vehicle emission standards to limit vehicle exhaust emissions, such as U. S. 2017–2025 Light-Duty Vehicle Greenhouse Gas Emissions Standards [15], Euro-6 Vehicle Standards [16] and China's Stage 6 Emission Standard for New Light-duty Vehicles [17]. However, for many big cities some pollution are inevitable and other measures should be adopted. Pollution transmission control has been used for a long history, such as road sweeping and water spraying, which are still the main means of beautifying the environment. However, they are difficult to implement in crowded places and sprinkling could make the road slippery in winter. In recent years, researchers proposed some passive control strategies to alter the pollutant dispersion patterns, including the use of urban vegetation [18,19], noise barriers [18,20], low boundary wall [21], on-street parked car [22] and so on. The goal is to reduce air pollution concentrations for pedestrians by increasing local pollution in other places. These passive control strategies are seen as promising for improving air quality in urban street canyons, but such strategies are better to be integrated with the urban planning [23]. For established public area big changes may be required in existing public facilities, in addition most of passive control only change the distribution of pollutants without removing them.

This paper provides another strategy to mitigate the air pollution in the street canyons by adding purifying devices to municipal equipment and making them "actively" remove pollutant in the street canyons. We design a novel air cleaning street lamp, which integrates the functions of illumination and purification. Street lamps are an important feature of urban street canyons. Air cleaning street lamps will not change the original urban planning, they are placed on both sides of the road, hence they can directly purify vehicle exhaust to improve the air quality of the street canyons. A typical street canyon with an aspect ratio of H/W = 1, which is not easily ventilated, is studied. The purpose of this paper is to study how to mitigate automobile exhaust pollution of fuel vehicles in urban street canyons. The pollution in the street canyon under three approaching wind directions (perpendicular, oblique and parallel wind directions) and five wind speeds (0.90 $m{\cdot}s^{-1}$, 2.45 $m{\cdot}s^{-1}$, 4.40 $m{\cdot}s^{-1}$, 6.70 $m{\cdot}s^{-1}$ and 9.35 $m{\cdot}s^{-1}$ based on Beaufort scales 1–5, see supplementary material) are studied. Three major aspects are investigated. Firstly, pollution in street canyons is studied. The impact of China 6b Light-duty Fuel Vehicle Emission Standard fully implemented in 2023 [17] on the improvement of air quality in the street canyon is analyzed by comparing with China 5 Light-duty Fuel Vehicle Emission Standard [17]. Then, the effects of four different types of air cleaning street lamps are discussed. Finally, the purification effects of emission reduction measures and air cleaning street lamps are compared.

The rest of this paper is arranged as follows. Section 2 introduces the street canyon models. The numerical method is presented and validated in Sections 3. Section 4 shows some results of applying emission reduction measures and air cleaning street lamps to the street canyon. Section 5 presents limitations and further study. Finally, some conclusions are drawn in Section 6.

2. Street canyon models

2.1. The experimental street canyon model in the wind tunnel

The experimental street canyon model used to verify the numerical method is from CODASC [24], as shown in Fig. 1. CODASC is a database that provides traffic pollutant concentrations in urban street canyons obtained from wind tunnel dispersion experiments. The experimental street canyon model is composed of two parallel aligned blocks made of acrylic glass with length to height ratio L/H = 10 and the aspect ratio of

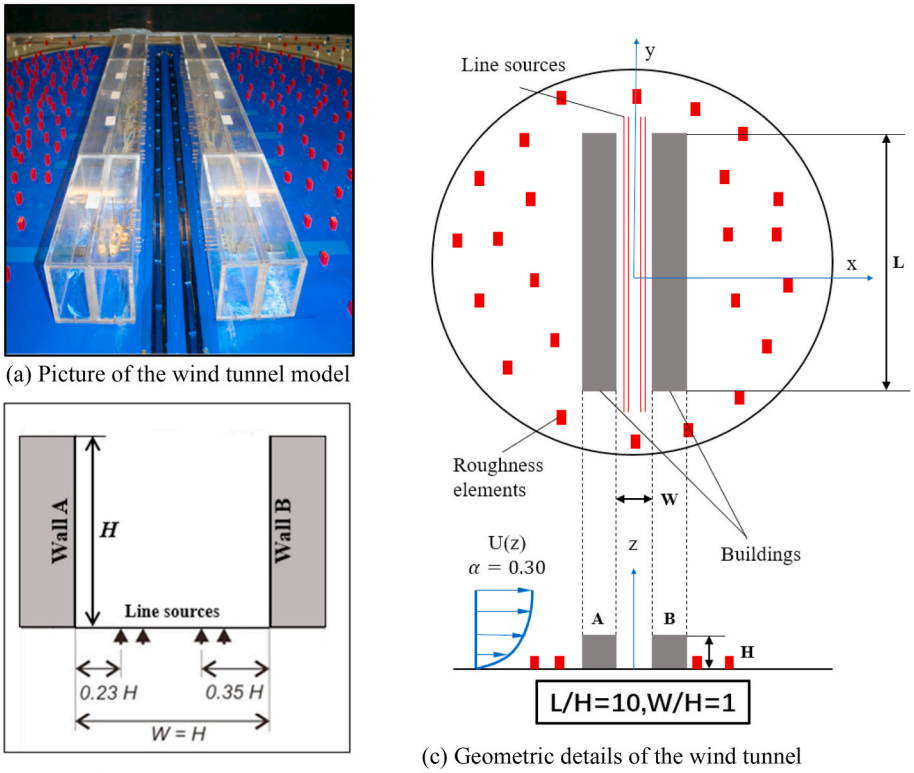

(a) Picture of the wind tunnel model

(b) Line sources position

(c) Geometric details of the wind tunnel

Fig. 1. The street canyon model from CODASC [24].

street width to building height W/H = 1(Fig. 1). As it can be seen from Fig. 1 there are many small roughness elements outside the street canyon. Such a setup is used to simulate urban atmospheric boundary layer of model at scale of 1:150. The building models have dimensions $L \times W \times H = 1.2\ m \times 0.12\ m \times 0.12\ m$, corresponding to $L \times W \times H = 180\ m \times 18\ m \times 18\ m$ in full scale. In the test section, a typical urban boundary layer flow with mean velocity profile exponent $\alpha_u = 0.30$ and turbulence intensity profile with exponent $\alpha_I = 0.36$ are reproduced according to the power law shown below [25]:

$$\frac{u(z)}{u(z_{ref})} = \left(\frac{z}{z_{ref}}\right)^{\alpha_u}, \tag{1}$$

$$\frac{I_u(z)}{I_u(z_{ref})} = \left(\frac{z}{z_{ref}}\right)^{-\alpha_I}, \tag{2}$$

where, $u(z_{ref})$ is the reference wind velocity equal to 4.70 $m{\cdot}s^{-1}$ at the top of the building (z = H), and z_{ref} is the reference length equal to the building height.

Four-line sources at an emission rate of 10 $g{\cdot}s^{-1}$ with sulphur hexafluoride (SF_6) as tracer gas are installed at street canyon center lines and the line sources are exceeded approximately by 10% at street entrance and exit to consider the traffic emissions of street intersections.

An electron capture detection (ECD) is employed to detect and analyze the concentration distribution of SF_6. Concentration distribution is measured at the canyon walls and normalized according to

$$C^{+} = \frac{cu_H H}{Q/l}, \tag{3}$$

where c is the measured concentration, u_H is the inflow velocity at height H and Q/l is the mass emission rate per unit length.

2.2. The street canyon model with street lamps

Street lamps are the typical feature of urban street canyons. In this paper, a new full scale street canyons model with street lamps is established based on CODASC's street canyon model, as shown in Fig. 2. A total of 38 street lamps are evenly spaced along the street with 10 m intervals. For the convenience of modeling and grid division, the street lamp is designed as a cuboid with the length, width and height of 0.3 m, 0.3 m and 3.5 m, respectively. The street canyon is divided into two pedestrian streets and a two-lane road by the two rows of street lamps. Pedestrian street A near Wall A and pedestrian street B near Wall B are 3 m wide, and the middle road is 12 m wide. The breathing zones of the pedestrian at height from 1.5 m to 1.8 m are shown by the shaded area in Fig. 2(a). The pollutant concentrations of breathing zones are the major concern of this study.

The present authors put forward and designed a kind of air cleaning street lamps. Fig. 3(a) shows a prototype of the air cleaning street lamp installed in the Xi 'an Expo Park, in China. The bottom shell of the street lamp is perforated to allow polluted air to enter the purifying unit, and the purified air is blown out from the air outlets at the top of the street lamp. The purifying unit consists of a dust removal module, a catalytic oxidation module, and a fan, as shown in Fig. 3(b). The fan provides power to extract polluted air into the street lamp. Polluted air first goes through the high-efficiency dust removal module to remove particulate matters in the air, and then enters the catalytic oxidation module to remove some gaseous pollutants. Here, the high efficiency dust removal module adopts a high efficiency particulate air (HEPA) filter. HEPA has the advantage of high particle separation efficiency, but it has some disadvantages such as high costs and not suitable for high-temperature working conditions. The catalytic oxidation module adopts the catalyst supported by activated carbon (AC), which can be granular

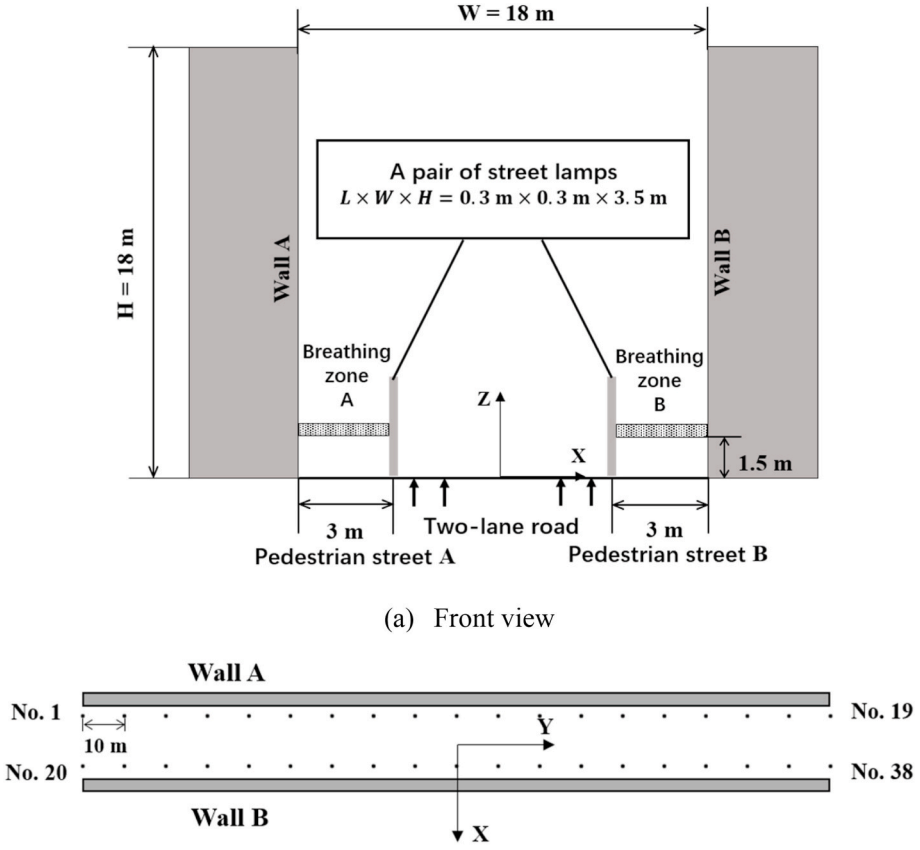

Fig. 2. The street canyon model with street lamps (the origin of the coordinates lies in the center of the street canyon).

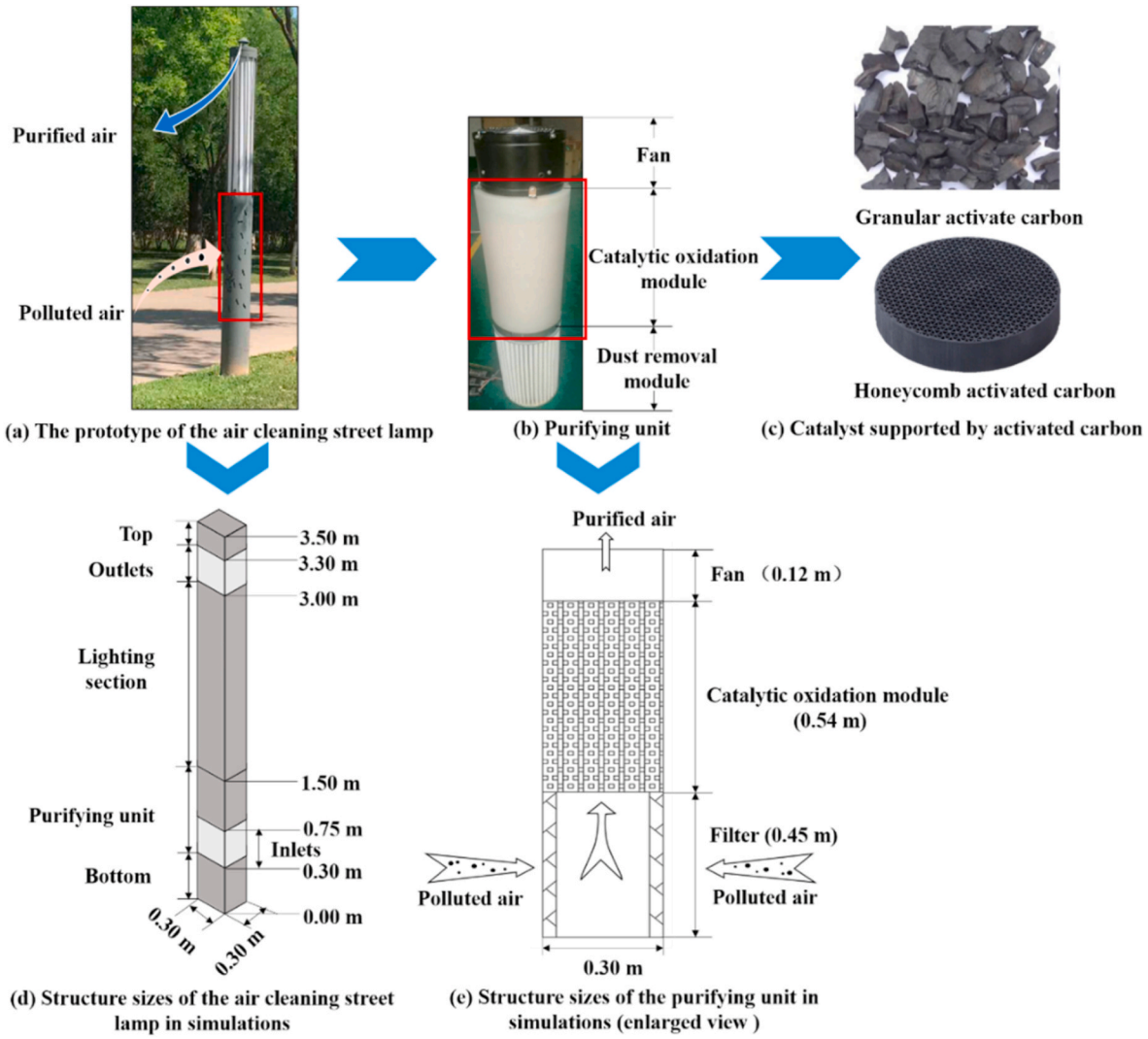

Fig. 3. Air cleaning street lamp prototype and physical model in simulations.

activated carbon or honeycomb activated carbon, as shown in Fig. 3(c). In practical application, the pressure-drop generated by the stacked granular activated carbon is larger than that generated by the honeycomb activated carbon with the same height, so the fan consumes more energy. Activated carbon can adsorb and remove fine particles and some gaseous pollutants in the air, and the supported catalyst can mineralize NO_x and degrade O_3 to produce non-toxic and harmless substances such as nitrate, water and carbon dioxide. For this prototype, activated carbon was self-doped by TiO_2 nanocomposite film, and TiO_2/AC was used as the catalyst. Detailed information about TiO_2 nanocomposite film can be found elsewhere [26]. The pollutant removal efficiency of the prototype was determined by the co-author Huang Yu's team by sampling the inlet and outlet air of the air cleaning street lamps. For a sampling period of seven days, the mass concentrations of $PM_{2.5}$ and O_3 of the inlet and outlet were hourly recorded through MAS (Mini Air Station) – AF - 200 (SAPIENS Environmental Technology, Shenzhen, China). Teflon air bags were used to collect the inlet and outlet air for NO_x analysis, and NO_x was measured by a chemiluminescence NO_x analyzer (Ecotech, Model 9841, Australia). They found that the removal efficiency of $PM_{2.5}$ can reach more than 80%, O_3 removal efficiency is greater than 50%, NO_x removal efficiency is greater than 50% in sunny days, and is greater than 30% in rainy days [27].

In this paper, the purification effect of air cleaning street lamps on pollution in the street canyon is studied by numerical simulation. Referring to the size of conventional street lamps and the structure of air cleaning street lamps, Fig. 3(d) shows the geometric details of the air cleaning street lamp in the numerical simulations and the structure of the purifying unit is shown in Fig. 3(e). The air cleaning street lamp is 0.30 m long, 0.30 m wide and 3.50 m high. It consists of the bottom, the purifying unit, the lighting section, the air outlet and the top. The purifying unit is simplified as a cuboid like the shell of the street lamps and installed at a height of 0.30 m. The air inlet of the purifying unit corresponds to the filter position in Fig. 3(e), with a height range of 0.30 m–0.75 m, which is also the height of most vehicles' exhaust emissions. The catalytic oxidation section of the purifying unit is supported by a honeycomb activated carbon, with a total height of 0.54 m. The air purified by purifying unit is blown to the environment from the air outlets set at the top of the air cleaning street lamp with a height range of 3.00 m–3.30 m, as shown in Fig. 3(d).

3. Numerical method

3.1. Mathematical formulation

In this study, a steady state Reynolds-averaged Navier-Stokes (RANS) model provided by the commercial CFD software FLUENT is employed to simulate the airflow in the street canyon. The governing equations for the conservation of mass and momentum can be written as:

$$\frac{\partial U_i}{\partial x_i}=0, \tag{4}$$

$$U_j\frac{\partial U_i}{\partial x_j}=-\frac{1}{\rho}\frac{\partial P}{\partial x_i}+\nu\frac{\partial^2 U_i}{\partial x_j\partial x_j}-\frac{\partial}{\partial x_j}\left(\overline{u_i'u_j'}\right), \tag{5}$$

here x_i indicates the ith Cartesian coordinate (i = 1,2,3), U_i (m·s^{-1}) indicates the time-averaged velocity component, u_i' is the fluctuation from the ith mean velocity component, and $\overline{u_i'u_j'}$denotes the Reynolds stresses and its determination depends on what turbulence model is adopted.

Based on the previous investigations [28,29], the standard k-ε turbulence model is adopted. Transport equations for the turbulent kinetic energy, k and turbulent kinetic energy dissipation rate, ε can be described as

$$U_j\frac{\partial k}{\partial x_j}=\frac{\partial}{\partial x_j}\left[\left(\nu+\frac{\nu_t}{\sigma_k}\right)\frac{\partial k}{\partial x_j}\right]-\overline{u_i'u_j'}\frac{\partial u_i}{\partial x_j}-\varepsilon, \tag{6}$$

$$U_j\frac{\partial \varepsilon}{\partial x_j}=\frac{\partial}{\partial x_j}\left[\left(\nu+\frac{\nu_t}{\sigma_\varepsilon}\right)\frac{\partial \varepsilon}{\partial x_j}\right]-C_{\varepsilon 1}\frac{\varepsilon}{k}\overline{u_i'u_j'}\frac{\partial u_i}{\partial x_j}-C_{\varepsilon 2}\frac{\varepsilon^2}{k}, \tag{7}$$

and the Reynolds stress can be expressed by

$$\overline{u_i'u_j'}=\frac{2}{3}k\delta_{ij}-\nu_t\left(\frac{\partial u_i}{\partial x_j}+\frac{\partial u_j}{\partial x_i}\right), \tag{8}$$

where δ_{ij} represents the Kronecker delta, and ν_t (m^2·s^{-1}) is the turbulent viscosity that can be expressed as:

$$\nu_t=C_\mu k^2/\varepsilon \tag{9}$$

In the above equations, constants C_μ, $C_{\varepsilon 1}$, $C_{\varepsilon 2}$, σ_k and σ_ε are specified as 0.09, 1.44, 1.92, 1.0 and 1.3, respectively [30,31].

Considering the low concentration of automobile exhaust in the air and assuming that its motion does not affect turbulence, for the pollutant transfer in the street the scalar transport equation can be used [32–35]. Automobile exhaust contains gaseous pollutants and particulate matters. In the simulation of gaseous pollutants, it is assumed that gaseous pollutants are stable and do not participate in chemical reactions. In the simulation of particulate matters, considering the settlement caused by gravity influence the drift flux model is used [36,37]. The transport equations of gaseous pollutants and particulate matters are shown respectively below:

$$\frac{\partial\left(U_jC_g\right)}{\partial x_j}=\frac{\partial}{\partial x_j}\left[\left(D_{m,g}+\frac{\nu_t}{Sc_{t,g}}\right)\frac{\partial C_g}{\partial x_j}\right] \tag{10}$$

$$\frac{\partial\left[\left(U_j+U_{j,s}\right)C_p\right]}{\partial x_j}=\frac{\partial}{\partial x_j}\left[\left(D_{m,p}+\frac{\nu_t}{Sc_{t,p}}\right)\frac{\partial C_p}{\partial x_j}\right] \tag{11}$$

here the variable C (kg·m^{-3}) represents the mass concentration of pollutants, the subscript g represents gaseous pollutants, and p represents particulate matters. D_m (m^2·s^{-1}) is the molecular diffusion coefficient for the pollutants, Sc_t is the turbulent Schmidt number, and $U_{j,s}$ (m·s^{-1}) is the settling velocity of particulate matters. Sc_t has a significant impact on the simulation of pollutant concentration [38,39]. In this paper, Sc_t is chosen equal to 0.3 consistent with Gromke's study [25] for the perpendicular wind direction and 0.7 for the oblique and parallel wind direction. $U_{j,s}$ can be expressed by the following formula [40]:

$$U_{j,s}=\frac{\rho_p d_p^2 g}{18\mu} \tag{12}$$

here ρ_p is the density of the particle, kg·m^{-3}, d_p is the diameter of the particle, μm, g is the gravitational acceleration, m·s^{-2}. The settling velocity is always in the same direction as gravity, that is, perpendicularly downward.

For the convenience of presentation, the boundary conditions will be provided in the next section.

3.2. Numerical simulation setup

3.2.1. Computational domain

Three different computational domains are created based on different wind directions. We use θ as the angle between the street canyon axis and the wind direction. Perpendicular, oblique and parallel wind directions correspond to θ = 90°, 45° and 0°, respectively (see Fig. 4). Under the guideline of COST ACTION 732 [41], we set the street canyon 8H away from the inlet of the computation domain, 10H away from the laterals, 30H away from the outlet and the total height of the computation domain is 8H. Fig. 4 gives the computation domain and boundary conditions for perpendicular, oblique and parallel wind direction. The sub-domain is a box with 12 H × 5 H × 2H tightly surrounded the street canyon that is the most interesting region in this study. In Fig. 4 the origin of the coordinates lies in the center of the street canyon (see Fig. 2), the coordinate Y is always parallel to the street and Z is vertical to the ground.

3.2.2. Meshing strategy

In simulations, the full scale street canyon ($L \times W \times H$ = 180 × 18 × 18 m^3) is adopted and the same grid is used for the street canyon with or without street lamps. Compared with the dimension of the street canyon and the overall calculation domain, the street lamp size ($L \times W \times H$ = 0.3 × 0.3 × 3.5 m^3) is very small. In order to reflect the influence of street lamps on the airflow in the street canyon, the horizontal grid spacing of street lamps is 0.075 m. The vertical grid spacing is 0.1 m, except that the first layer grid is 0.3 m in consideration of the surface roughness. The grid-step expansion ratio is below 1.2 in the whole computational domain. Structured grids are used in the whole computational domain when the wind direction perpendicular and parallel to the street canyon axis. However, when the wind direction is 45° the structured grids are used in the sub-domain and unstructured grids are generated in the rest to guarantee the grid quality. A grid sensitive analysis has been performed in the supplementary material (see Fig. S2.1-2 in the supplementary material). Finally, the total cells are about 3219178, 3519930 and 3050127 for θ = 90°, 45° and 0°, respectively. The computational grid for each wind direction and detailed grid views of the canyon inlet and street lamps can be seen in Fig. S3.1-2 in the supplementary material.

3.2.3. Boundary conditions and solution method

As shown in Fig. 4, the two sides and the top of the calculation domain are symmetric boundaries. Pressure outlet boundary is adopted at the outlet of the calculation domain.

The inlet velocity boundary condition takes two practices. Firstly, the numerical model is verified by the wind-tunnel experiments, so the approaching profiles measured from the wind-tunnel model are used at the inlet of the calculation domain. The inlet velocity profile is determined by Eq. (1), and the turbulent kinetic energy and the dissipation rate are specified as below [24]:

$$k=\frac{u_*^2}{\sqrt{C_\mu}}\left(1-\frac{z}{\delta}\right), \tag{13}$$

$$\varepsilon=\frac{u_*^3}{\kappa z}\left(1-\frac{z}{\delta}\right), \tag{14}$$

where u_* is the friction velocity and is equal to 0.52 m·s^{-1}, δ is the boundary layer thickness and is equal to 144 m, and κ is the von Kàrmàn constant and is equal to 0.40.

Then for the study of the street canyon under different ambient wind speeds, the fully developed inlet profile under neutral atmospheric boundary proposed by Richards and Hoxey [42] is adopted, as shown below:

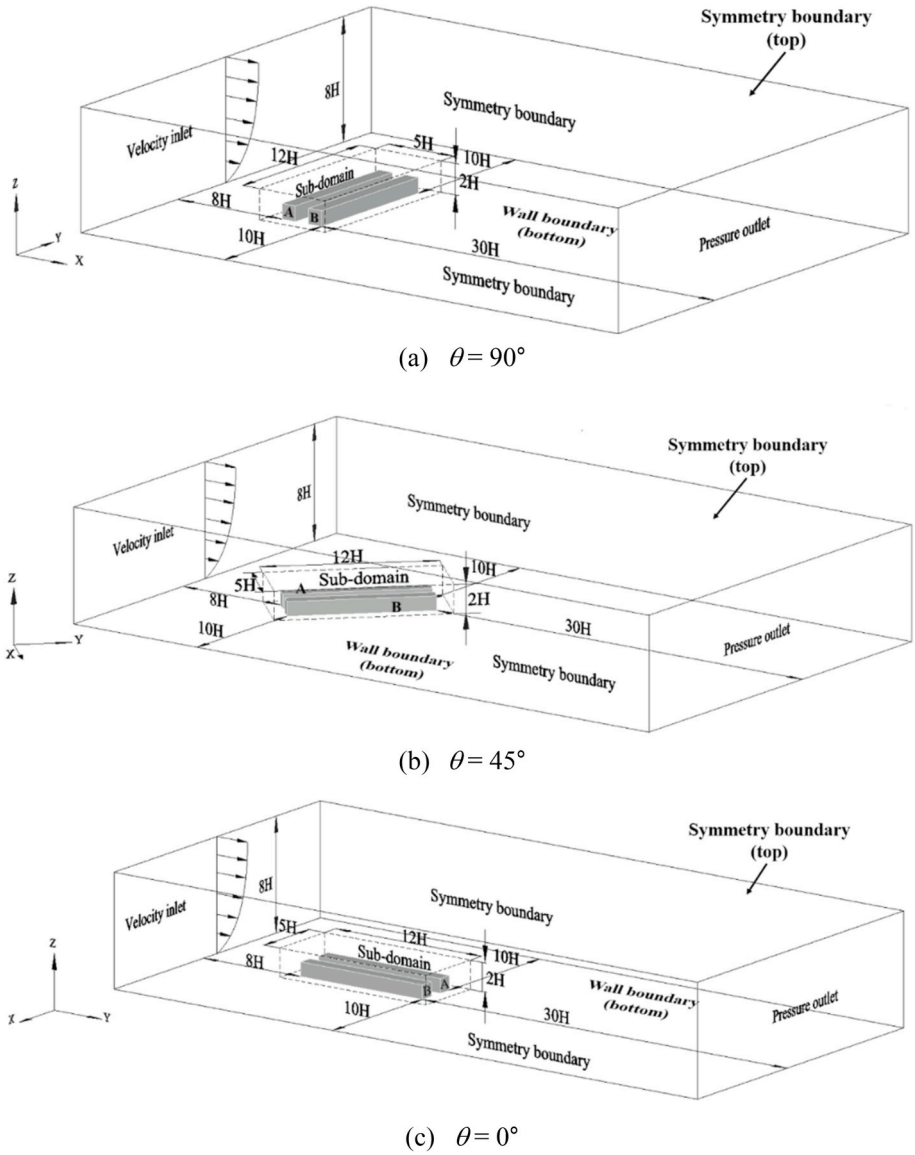

Fig. 4. Computation domains and boundary conditions for perpendicular, oblique and parallel wind direction (the origin of the coordinates lies in the center of the street canyon, see Fig. 2).

$$u = \frac{u_*}{\kappa}\ln\left(\frac{z+z_0}{z_0}\right) \tag{15}$$

$$k = \frac{u_*^2}{\sqrt{C_\mu}} \tag{16}$$

$$\varepsilon = \frac{u_*^3}{\kappa(z+z_0)} \tag{17}$$

where C_μ is the coefficient in turbulence model (0.09). The ambient wind speeds are selected according to the Beaufort scale. The intermediate values for each wind level are selected as the inlet wind speed at z = 10 m (see Table S1 in the supplementary material). The friction velocity u_* is first calculated according to Eq. (15) and the selected wind speed at $z = 10$ m, and then u_* is put into Eqs. (15–17) to determine the inlet wind profile of the calculation domain.

No-slip wall boundary conditions are imposed on the ground surfaces inside and outside the sub-domain. But, the ground surfaces outside the sub-domain should consider the influence of rough elements as shown in Fig. 1, so the modified wall function is adopted [43], as shown below:

$$k_s = \frac{9.793 z_0}{c_s} \tag{18}$$

where k_s is the equivalent roughness height, c_s is the roughness constant, and z_0 is the aerodynamic roughness length. In the present study, z_0 is

Table 1
Comparison of emission limits of China 5 and China 6b.

	CO mg·km^{-1}	THC mg·km^{-1}	NMHC mg·km^{-1}	NO_x mg·km^{-1}	N_2O mg·km^{-1}	PM mg·km^{-1}	PN #·km^{-1}
China 5	1000	100	68	60	NA	4.5	NA
China 6b	500	50	35	35	20	3	6×10^{11}

specified to 0.1 m referring to Ref. [32] that represents rough and open terrain like agricultural land with scattered buildings, k_s is equal to 0.12 m which is less than half of the height of ground-adjacent cells, so the roughness constant c_s is chosen equal to 8.

For the buildings A and B, the no-slip wall boundary condition is used. The conventional street lamp is a solid cuboid and airtight, and the no-slip wall boundary condition is adopted for its surface in the simulations. The air cleaning street lamp has air inlets and air outlets, and the boundary conditions are presented in Fig. 5.

As shown in Fig. 5(a), in simulations the air cleaning street lamp is divided into two parts, the upper part and the lower part. The interior of the upper part is not participating in the simulation of the fluid zone, the no-slip wall boundary condition is used for the upper shell, and the upper air outlet is set as the velocity boundary condition. Outlet wind speed and pollutant concentration depend on the mass flow rate and purification efficiency of the purifying unit of the lower part. The lower part of the air cleaning street lamp is simulated as a fluid zone. The filter is the inlet of the polluted air and is represented by the porous jump boundary [31]. The catalytic module of honeycomb activated carbon is simulated as a porous medium region. The boundary condition of the fan outlet surface of the purifying unit is set as the exhaust fan boundary condition [31]. The lower shell of the air cleaning street lamp is set as no-slip wall boundary. We have designed four air outlet modes, as shown in Fig. 5(b). Design A has four horizontal air outlets. Design B has four 45° downward air outlets. Design C and Design D have one air outlet facing to the pedestrian streets only. Between them, Design C has one horizontal air outlet, and Design D has one 45° downward air outlet.

Experiments on the relationship between wind speed and pressure drop were carried out on the purifying unit of the prototype and the parameters are used as simulation parameters. The face permeability of the filter is 1.73×10^{-8} m^2, the porous medium thickness is 0.04 m, and the pressure loss coefficient is 733 m^{-1}. The catalytic module of honeycomb activated carbon has the viscous resistance coefficient 2.71×10^6 m^{-2}, the internal resistance coefficient 8 m^{-1} and the porosity 64%. According to the street lamp size and axial flow fan available in the market, the full pressure of the fan is set as 250 Pa. The user-defined functions (UDFs) are implemented to connect the air outlets and the purifying unit. According to the principle of mass conservation, the UDFs convert the air mass flow rate through the purifying unit into the wind speed of the air outlets, and convert the amount of pollutants, which is the total amount of pollutants flowing into the purifying unit minus the amount removed by the purifying unit, into the pollutant concentration of the air outlets.

As indicated above, in the simulations of wind tunnel experiments, SF6 is taken as the pollutant, and the emission intensity of the line sources is 10 g·s^{-1}. In the present study, China 5 Light-duty Vehicle Emission Standard and China 6b Light-duty Vehicle Emission Standard are compared. Table 1 shows the comparison of emission limits of China

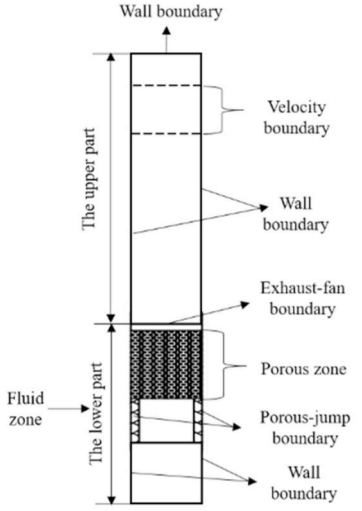

(a) Boundary conditions

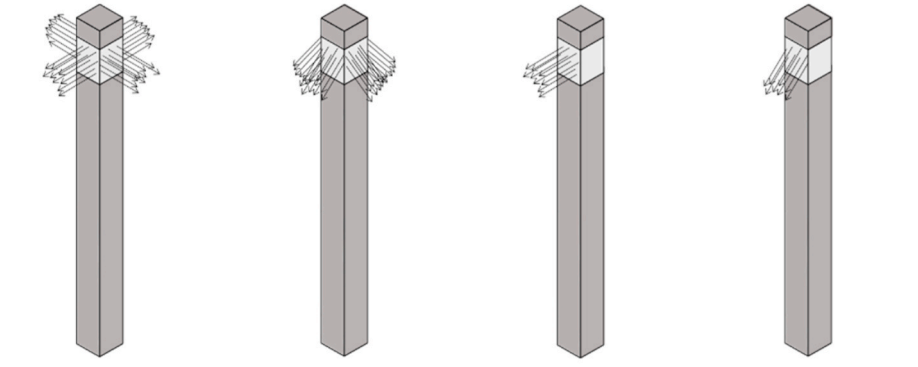

(b) Four air outlet designs

Fig. 5. Boundary conditions and air outlet designs of the air cleaning street lamp.

5 and China 6b standards, including carbon monoxide (CO), total hydrocarbons (THC), non-methane hydrocarbons (NMHC), nitrogen oxides (NO_x), nitrous oxide (N_2O), particulate matter (PM) and particle number (PN). However, the current air cleaning street lamps can filter PM, remove NO_x and degrade O_3. Therefore, PM and NO_x of the automobile exhaust are taken as the simulation objects in this paper. Considering that a considerable part of pollutants of the automobile exhaust cannot be purified but their influence cannot be ignored, hence CO is also taken as the simulation object which is the largest emission in the automobile exhaust. In numerical simulations, the removal rates of PM, NO_x and CO of the purifying unit are set to be 85%, 50% and 0% respectively. The largest emission gas CO that can not be purified by air cleaning street lamps has been studied. Therefore, the present work could, to a large degree, represent the effect of air cleaning street lamps on mitigation of automobile exhaust pollution.

The vehicle emission rates can be determined by the following formula:

$$Q_{jw} = \sum_{i}^{n} \left(N_{ji} \times Ef_{jw} \times L_i \right) \tag{19}$$

where Q is the emission rate for each vehicle class, j, and each type of pollutant, w, in mg·h^{-1}. N is the number of vehicle trips for each vehicle class, j, and each link, i, in veh·h^{-1}. Ef is the emission factor for each vehicle class, j, and each type of pollutant, w, in mg·(km·veh)$^{-1}$. L is the length of each link, i, in km.

In the simulation, it is assumed that all the motor vehicles in the street canyon are light-duty vehicle. Ef of PM, NO_x and CO is taken as the limit values listed in Table 1. Referring to the street canyon models in Fig. 2, the length of the line sources, L, is 216 m. As the movement of vehicles can also influence air pollution [44], the critical situation before queue formation in the lane is chosen. According to the research of Zavala-Reyes et al. [45], the critical capacity before queue formation is 14 veh·min^{-1} for a 220 m long road and for the typical speed of 50 km·h^{-1} in the city. In this study, the width of the middle road is 12 m and can be set to two-lane. Therefore, the number of vehicle trips, N, is taken as 28 veh·min^{-1}. In addition, in order to compare the air quality inside and outside the street canyon, the concentrations of PM, NO_x and CO at the inlet of the calculated domain are set as 35 μg·m^{-3},80 μg·m^{-3} and 10000 μg·m^{-3}, respectively.

The three-dimensional steady RANS equations, standard k-ε turbulence closure and the contaminant transport equations are solved with FLUENT 14.0. The SIMPLE algorithm is adopted to deal with the pressure-velocity coupling. Second-order upwind discretization scheme and the central difference discretization scheme are selected for convection term and diffusion term, respectively. The double precision solver is adopted. Multicore parallel UDFs are developed to simulate the purification of the air cleaning street lamps. In addition to numerical model verification, a total of 90 scenarios are simulated which cover following situations: street canyons without street lamps, with conventional street lamps, and with four different air cleaning street lamps, under three wind directions and five wind speeds.

3.3. Model validation

Based on the data of the normalized concentration C^+ provided by CODASC [24], Fig. 6 compares C^+ on Wall A and Wall B between measured data [24] and simulation results. The simulation results show a quite good qualitative agreement with measured data. To quantify the differences between the simulation results and test data, following metrics suggested by Chang and Hanna [46] are adopted:

$$\mathrm{FB(fractional\ \ bias)} = 2\frac{\overline{c_o} - \overline{c_p}}{\overline{c_o} + \overline{c_p}}, \tag{20}$$

$$\mathrm{NRMSE(normalized\ \ root\ \ mean\ \ square\ \ error)} = \sqrt{\frac{\overline{\left(c_o - c_p\right)^2}}{\overline{c_o} \cdot \overline{c_p}}}, \tag{21}$$

$$\mathrm{R(correlation\ \ coefficient)} = \frac{\overline{\left(c_o - \overline{c_o}\right)\left(c_p - \overline{c_p}\right)}}{\sigma_{c_o} \cdot \sigma_{c_p}}, \tag{22}$$

$$\mathrm{FAC2} = \mathrm{fraction\ \ of\ \ data\ \ that\ \ satisfy}\ 0.5 \le \frac{c_p}{c_o} \le 2.0, \tag{23}$$

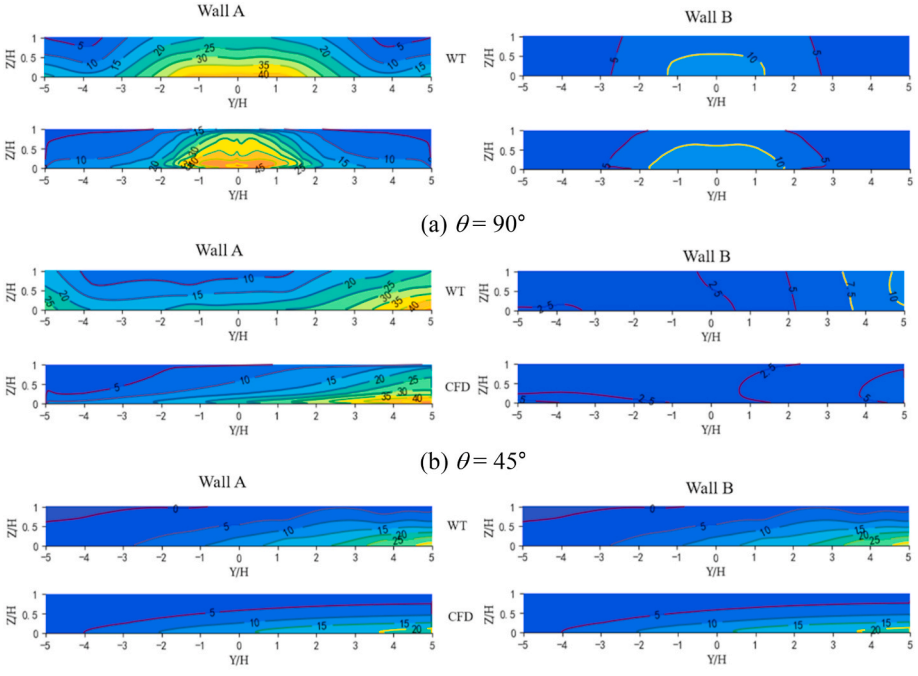

Fig. 6. Comparison of the normalized concentration C^+ on Wall A and Wall B between the wind tunnel experiments and numerical simulations.

here c_o refers to the observed value, c_p represents the predicted value, an overbar denotes the average of the data set, and σ means standard deviations.

Table 2 summarizes the statistical deviation results. The target value (Aim) and recommended criteria are shown. A perfect simulation should make all the metrics reach the target value, but it is obviously difficult to achieve a perfect simulation in practice, so Chang and Hanna gave the acceptable range of each metric in their research [46,47]. It can be seen that only for $\theta = 45°$ FB for Wall B is 0.374 (highlighted in the Table 2) and slightly beyond the recommended upper limit 0.3, and all other indicators are within the recommended ranges. The quantitative agreement between CFD results and wind tunnel data for $\theta = 45°$ is worse than that for $\theta = 90°$ and 0°, which is similar to the previous studies [32,48]. From the qualitative and quantitative analysis, for $\theta = 45°$ the normalized pollutant concentrations C^+ at Wall B is a bit underestimated. Such discrepancies may be caused by the k-ε turbulence model. Because for $\theta = 45°$ the flow pattern is characterized by strong rotating flow (see Fig. S.4.1 in the supplementary material). And it is the weakness of the adopted standard k-ε turbulence to predict such complicated flow [31]. But all trends observed in the wind tunnel experiments for $\theta = 90°$, 45° and 0° could be reproduced by the CFD simulations, and reasonably good quantitative agreement was obtained for most cases. Hence, the agreement between present simulation results and wind tunnel data should be considered satisfactory.

It can be seen from Fig. 6, for $\theta = 90°$ and 45°, the pollutants are concentrated on the Wall A side, for $\theta = 90°$ the middle of the street canyon have the highest concentration of the pollutant, and for $\theta = 45°$ the highest concentration of the pollutant is found at the exit of the street canyon. For $\theta = 0°$ the pollutant distributions of Wall A and Wall B are consistent and the highest concentration of the pollutant is found at the exit of the street canyon. With the improvement of ventilation condition in the street canyon, θ from 90° to 0°, the concentrations of the pollutant decrease gradually.

4. Results and discussion

4.1. Analysis of the street canyon with street lamps without air cleaning function

Calculations in this section are based on China 5 standard. The influence of conventional street lamps on automobile exhaust diffusion is analyzed. Take PM distribution at z = 1.65 m under force Beaufort 3 (4.4 m·s^{-1}) as an example, as shown in Fig. 7. The region at the range of $-0.50 \leq X/H \leq -0.34$ is in the breathing zone A and the range of $0.34 \leq X/H \leq 0.50$ is in the breathing zone B (the location of the breathing zones is shown in Fig. 2(a)). Because the street lamps increase local flow resistance hence weaken the air flow there leading to some local suppression of pollutants dispersion. From Fig. 7, it can be seen that at some zones the conventional lamps can cause higher PM concentration. For $\theta = 90°$, in the middle of the street canyon, PMs in breathing zone A are increased, while PMs in breathing zone B are slightly reduced. For $\theta = 45°$, PMs in breathing zone A at the end of the street canyon increase significantly, while PMs in breathing zone B at the inlet of the street canyon decrease slightly. For $\theta = 0°$, because street lamps are located between the lanes and pedestrian streets as barriers, PMs are trapped in the road and decrease in breathing zones A and B at the end of the street canyon. After adding the conventional street lamps, the change of concentrations of NO_x and CO is consistent with that of PM, and is not

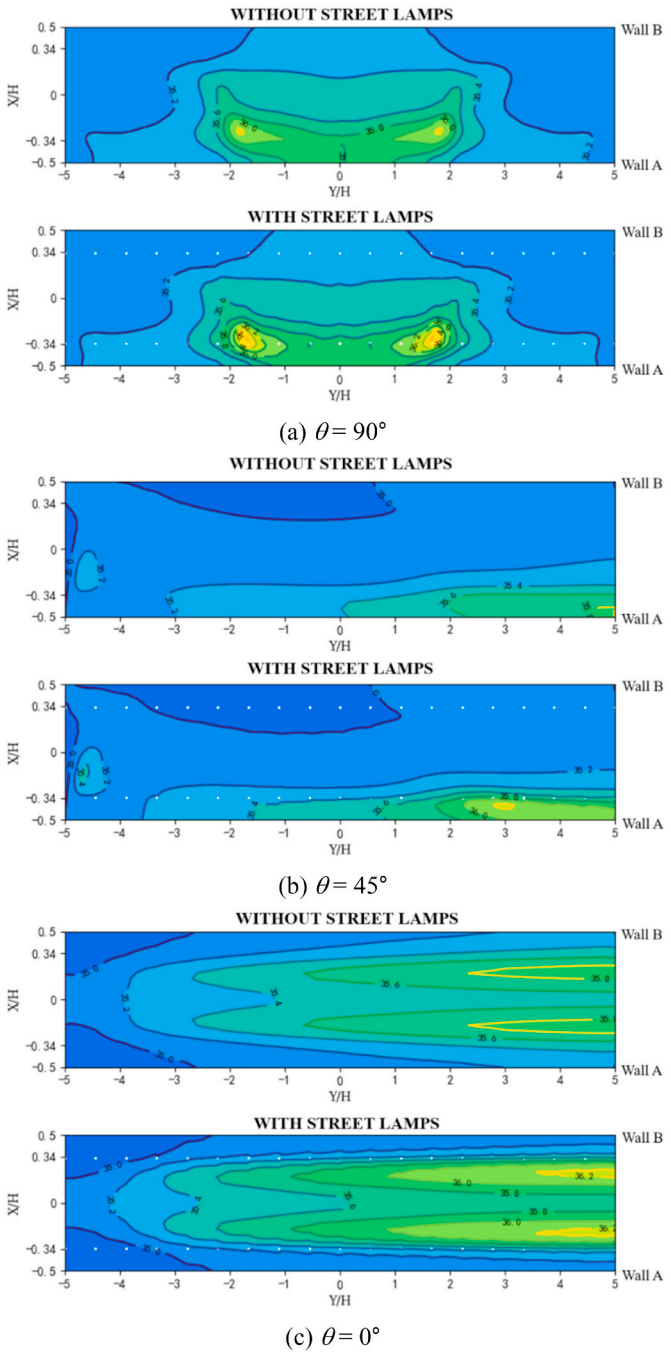

Fig. 7. Comparison of PM concentration inside the street canyon between cases without street lamps and with conventional street lamps, at the pedestrian height, 1.65 m, under force Beaufort 3 (4.4 m s^{-1}).

Table 2
The statistical deviation results for Wall A and Wall B at different wind directions.

Metric	Aim	Recommended criteria	$\theta = 90°$		$\theta = 45°$		$\theta = 0°$
			Wall A	Wall B	Wall A	Wall B	Wall A/B
FB	0	[−0.3,0.3]	0.157	−0.005	0.213	0.374	0.086
NRMSE	0	<1.225	0.351	0.149	0.408	0.706	0.386
FAC2	1	>0.5	0.911	0.983	0.724	0.779	0.796
R	1	>0.8	0.898	0.977	0.885	0.817	0.951

repeated here for simplicity.

Next, for the street canyon with conventional street lamps, the effects of approaching wind direction and speed on PM, NO_x and CO concentrations of breathing zones are analyzed. Fig. 8 shows the mean PM, NO_x and CO concentrations in breathing zones A and B under different wind directions and speeds. The mean concentrations of PM, NO_x and CO outside the street canyon are 35 μg·m^{-3}, 80 μg·m^{-3} and 10000 μg·m^{-3}, respectively, shown as red dotted lines. It can be seen that three pollutants clearly cross the thresholds (as red dotted lines) under force Beaufort 1 (0.90 m·s^{-1}), that means the air quality inside the street canyon is clearly worse than that outside the street canyon. With the increase of Beaufort force, the pollutant concentration inside the street canyon is more and more close to but still higher than the three thresholds, indicating that the air quality inside the street canyon is always worse than that outside the street canyon. The breathing zone A is the high-pollution zone, and under the same wind speed the concentration of PM, NO_x and CO is the lowest for $\theta = 0°$compared with the other two wind directions. The worst case happens under force Beaufort 1 (0.90 m·s^{-1}), and compared with the mean pollutant concentration outside the street canyon, for $\theta = 90°$, 45° and 0°, the mean PM concentration of breathing zone A increases by 7.66%, 8.50% and 2.63%, respectively; the mean NO_x concentration of breathing zone A increases by 59.43%, 65.81% and 33.81%, respectively; the mean CO concentration of breathing zone A increases by 7.92%, 8.77% and 4.51%, respectively; the mean PM concentration of breathing zone B increases by 1.43%, 0.003% and 2.63%, respectively; the mean NO_x concentration of breathing zone B increases by 13.95%, 4.20% and 33.81%, respectively; the mean CO concentration of breathing zone B increases by 1.86%, 0.56% and 4.51%, respectively.

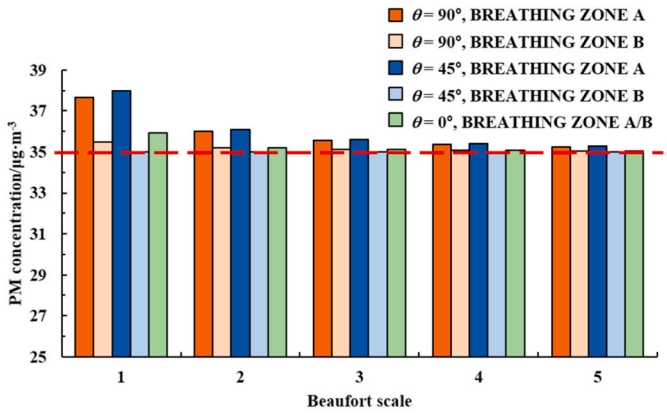

(a) Mean PM concentration

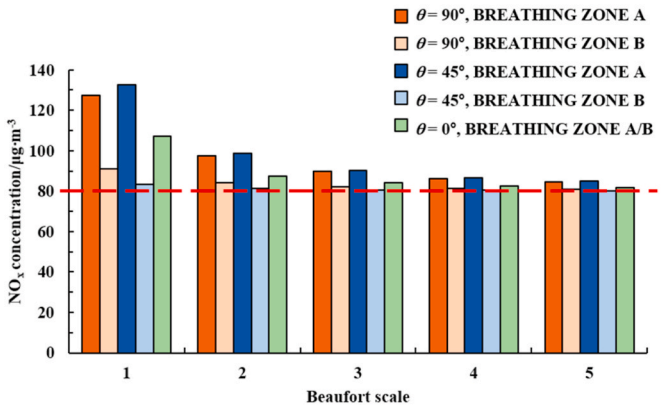

(b) Mean NO_x concentration

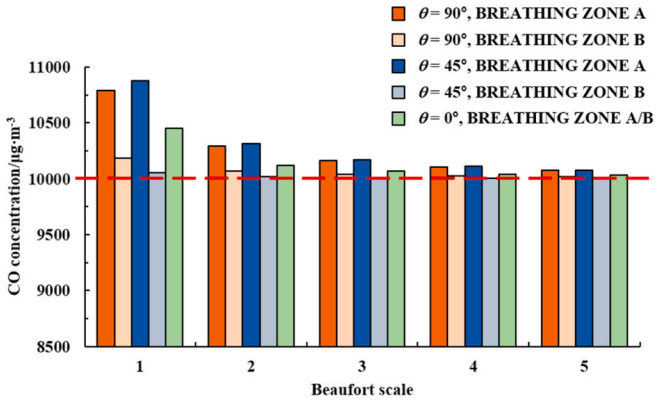

(c) Mean CO concentration

Fig. 8. Mean concentrations of three pollutants in breathing zones A and B under different wind directions and speeds (China 5).

4.2. Analysis of effect of reduced-emission

As seen in Table 1, the emission levels of China 6b standard are significantly lower than those of China 5 standard. Fig. 9 shows the simulation results based on this new standard for the mean PM, NO_x and CO concentrations in breathing zones A and B under different wind speeds and directions. Similar to the results shown in Fig. 8, at the same wind speed, compared with $\theta = 90°$ and 45°, the breathing zone A is less polluted for $\theta = 0°$; with the increase of wind speed, the pollutant concentrations in the street canyon are closer to the pollutant concentrations outside the street canyon, but still higher than that outside the street canyon. Even though the street canyon is still an area with poor air quality for the overall environment, however, comparing Figs. 8 and 9, it can be seen that reduced emission makes the pollutant concentrations of breathing zones decrease appreciably at lower wind velocity under the same other conditions. Under force Beaufort 1 (0.90 m·s^{-1}), by reducing vehicle emission from China 5 to China 6b in the street canyon for $\theta = 90°$, 45° and 0°, mean PM concentration of breathing zone A decreases by 3.11%, 3.42% and 1.86%, respectively; mean NO_x concentration of breathing zone A decreases by 15.53%, 16.54% and 10.53%, respectively; mean CO concentration of breathing zone A decreases by 3.67%, 4.03% and 2.16%, respectively; mean PM concentration of breathing zone B decreases by 0.78%, 0.24% and 1.86%, respectively; mean NO_x concentration of breathing zone B decreases by 5.09%, 1.68% and 10.53%, respectively; mean CO concentration of breathing zone B decreases by 0.91%, 0.28% and 2.16%, respectively. But pollutants are not only from the vehicle emissions but also from the outside of the street canyon. With increasing wind speed, more pollutants outside the street canyon are flowing into the street canyon, and the efficacy of reduced emission becomes less obvious, as can be seen from Figs. 8 and 9 for the last two force Beaufort cases.

It is interesting to note that comparing the results of China 5 and China 6b by dimensionless quantity such as defined by Eq. (3) is not feasible because China 5 and China 6b have different reference values.

4.3. Analysis of the street canyon with street lamps with air cleaning function

Here the effects of the air cleaning street lamp with different air outlet designs (as shown in Fig. 5) on the improvement air quality in the street canyon are compared and calculations in this section are based on the source level from China 5. Considering that the pedestrian breathing zones are below the air outlet height, Designs B and D are designed to flow downward. Designs C and D blow all purified air into the pedestrian streets to achieve the maximum impact on the pedestrian breathing zones. The air outlet height of the air cleaning street lamp is more than 3 m, for Designs C and D with one outlet the wind speed is about 4.8 m·s^{-1}, while for Designs A and B with four air outlets the wind speed of each

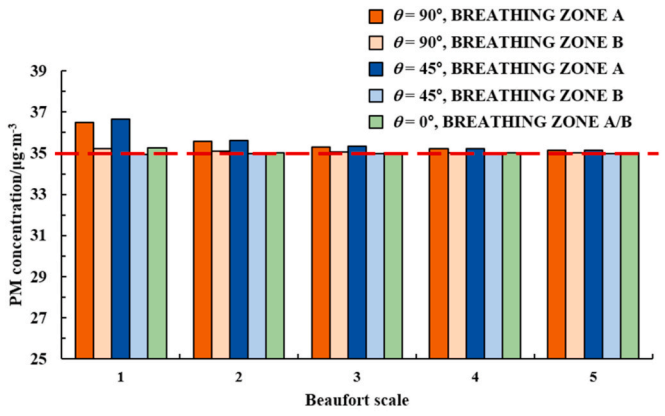

(a) Mean PM concentration

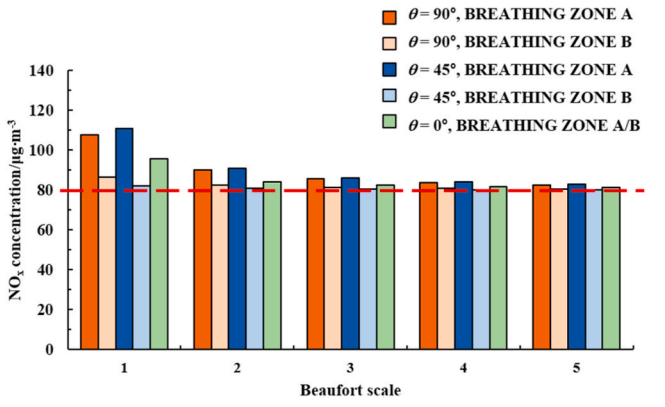

(c) Mean NO_x concentration

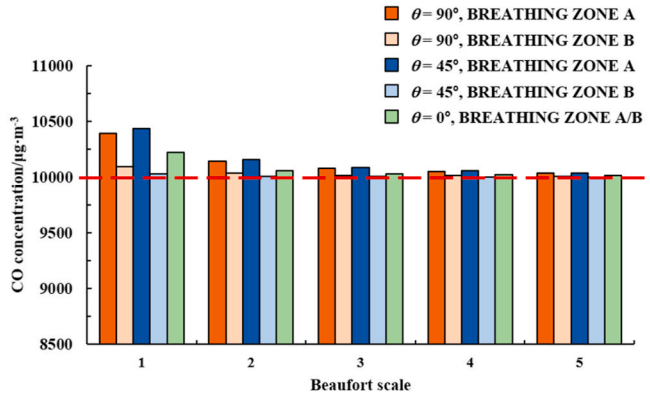

(c) Mean CO concentration

Fig. 9. Mean concentrations of three pollutants in breathing zones A and B under different wind directions and speeds (China 6b).

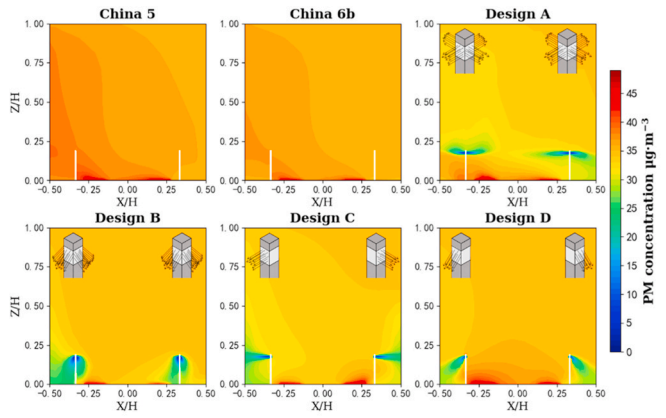

(a) $\theta = 90°$

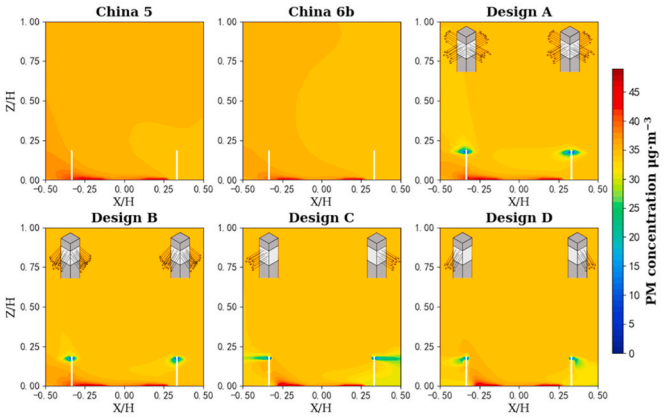

(b) $\theta = 45°$

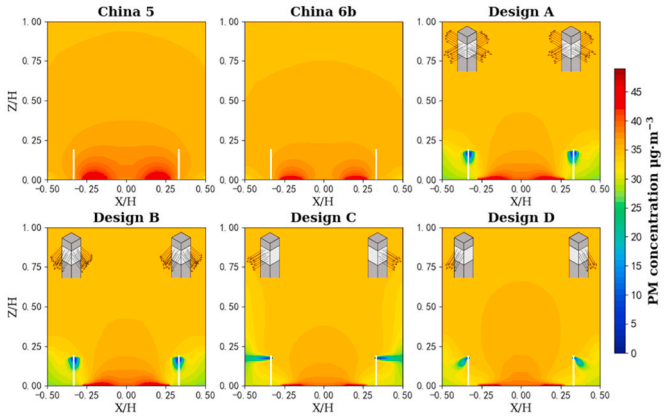

(c) $\theta = 0°$

Fig. 10. The PM concentration distribution in the central vertical cross section of the street canyon (Y = 0).

outlet is about 1.2 $m \cdot s^{-1}$, therefore, for the lower pedestrian areas, the air cleaning street lamps will not cause very uncomfortable experience for pedestrians.

When the approaching wind speed is high, pollutants inside the street canyon are mainly blown away by wind, but under lower wind speed air cleaning street lamps have an obvious effect of purification. Taking the cases under force Beaufort 1 (0.90 $m \cdot s^{-1}$) as examples, Fig. 10, 11 and 12 show the concentration distribution of PM, NO_x and CO at the vertical cross section of the street canyon. The four designs based on China 5, while the results based on China 6b with conventional lamps are also presented for comparison purpose. The bottom right and bottom left of each cloud image are pedestrian areas where we want to improve air quality. In the following the effects of air cleaning street lamps on the reduction of PM, NO_x and CO are analyzed individually. All the results are presented in dimensional quantities, since for pollution reduction study the major focus is on their absolute values.

First, look at the PM concentration distribution in the vertical cross section at middle of the street canyon, as shown in Fig. 10. The subfigure denoted by China 5 is the computational result based on the emission standard of China 5 with conventional street lamps, and it can be served as the comparison reference for evaluation of the effect of reduced emission based on China 6b and street lamps with air cleaning function. The PM removal rate of an air cleaning street lamp is 85%, and it can be found that under the three wind directions the PM concentrations in the

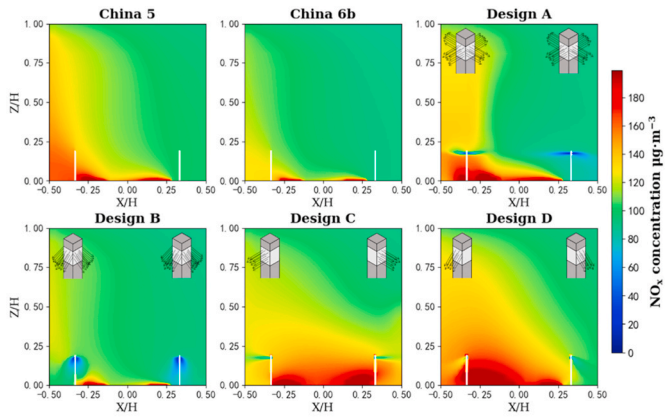

(a) $\theta = 90°$

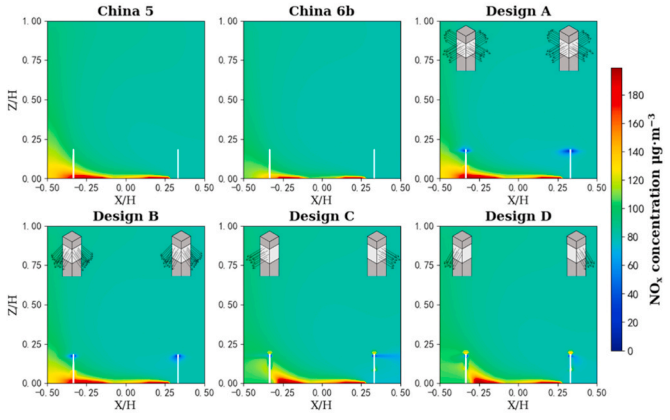

(b) $\theta = 45°$

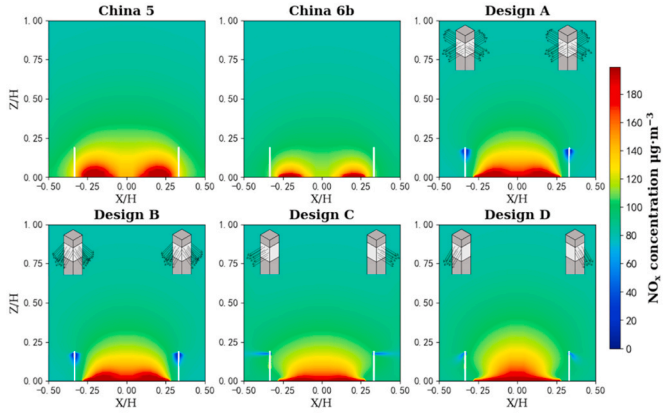

(c) $\theta = 0°$

Fig. 11. The NO_x concentration distribution in the central vertical cross section of the street canyon (Y = 0).

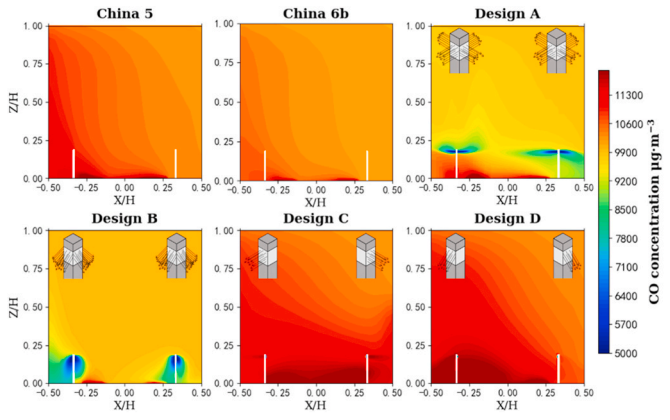

(a) $\theta = 90°$

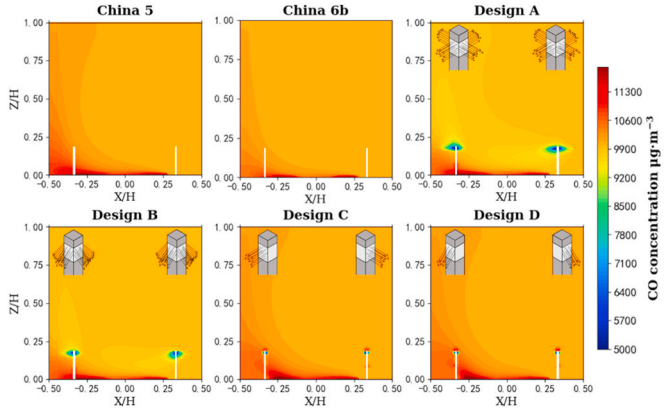

(b) $\theta = 45°$

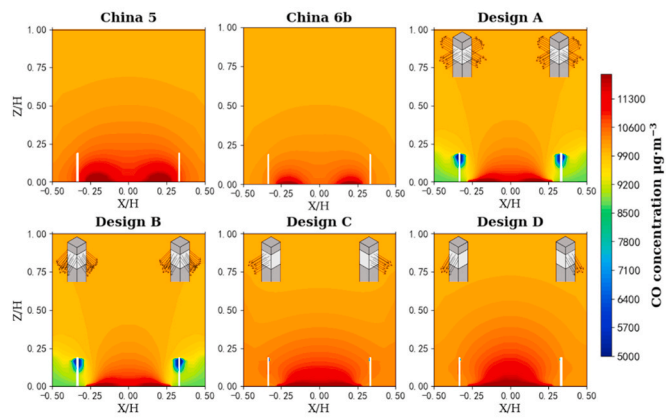

(c) $\theta = 0°$

Fig. 12. The CO concentration distribution in the central vertical cross section of the street canyon (Y = 0).

pedestrian areas are all significantly reduced by using air cleaning street lamps. A schematic diagram of the flow inside the street canyon under three wind directions is presented in Fig. S4.1 in the supplementary material. For $\theta = 90°$, a circulatory vortex is formed inside the street canyon. From the cloud map of Design A, it can be seen that the air from the right of the air cleaning street lamp is pressed down, while the air from the left air cleaning street lamp is lifted up. Therefore, Design A is not as good as the other three forms for PM reduction in the left pedestrian area. The air outlet speed of Design C is four times that of Design A, so the purified air can reach the left pedestrian area. Design B and Design D have better purifying effect due to the downward wind. After adding the air cleaning function for the street lamps, Designs A, B, C and D make the mean PM concentration of breathing zone A decrease by 5.96%, 11.68%, 13.73% and 14.61%, and make the mean PM concentration of breathing zone B decrease by 7.60%, 4.86%, 11.58% and 9.26%, respectively. For $\theta = 45°$, a spiral vortex along the canyon length is established. From the cloud map of Design C and Design D, it can be seen that the purified air of Design C and Design D is easy to reach the pedestrian areas due to the high speed of the air outlet. However, because purified air speed of Design A and Design B is smaller, the purified air may be rolled up and carried forward out of the street canyon by the spiral vortex. Therefore, PM reduction is not obvious in the pedestrian areas from the cloud map of Design A and Design B. Designs

A, B, C and D make the mean PM concentration of breathing zone A decrease by 4.10%, 4.62%, 13.12% and 14.19%, and make the mean PM concentration of breathing zone B decrease by 3.51%, 2.32%, 11.50% and 9.25%, respectively. For $\theta = 0^{\circ}$, wind moves horizontally along the street canyon, and four air outlet modes can all play a good purification effect on pedestrian areas. Designs A, B, C and D make the mean PM concentration of breathing zones A and B decrease by 13.27%, 16.95%, 12.20% and 12.27%, respectively.

Then, taking a look at the NO_x concentration distribution in the same section, and the results are shown in Fig. 11. From the cloud map of China 5, it can be found that the concentrations of NO_x at the bottom of the street near the pollution sources are significantly higher than that of other places in the street canyon. After reducing the emission of NO_x by the standard of China 6b, the NO_x concentrations in the pedestrian areas are significantly reduced. This indicates that the concentration of NO_x in pedestrian areas is more affected by vehicle exhaust emissions than by pollutants from outside the street canyon. The NO_x removal rate of an air cleaning street lamp is 50%. From the cloud maps, it can be observed that for $\theta = 90^{\circ}$, design B has the better purification effect. For the whole breathing zones, Designs A, B, C and D make the mean NO_x concentration of breathing zone A decrease by 4.67%, 11.29%, 16.92% and 13.78%, respectively, and make the mean NO_x concentration of breathing zone B decrease by 9.52%, 6.23%, −8.14% and −1.6%, respectively; for $\theta = 45^{\circ}$ designs C and D have a bit better purification effects than those of designs A and B. Designs A, B, C and D make the mean NO_x concentration of breathing zone A decrease by 3.81%, 6.59%, 19.22% and 18.89%, respectively, and make the mean NO_x concentration of breathing zone B decrease by 3.65%, 2.49%, 6.48% and 5.40%, respectively; for $\theta = 0^{\circ}$ the purification effects of Designs A and B are better than that of D which is better than Design C. Designs A, B, C and D make the mean PM concentration of breathing zones A and B decrease by 22.68%, 24.20%, 12.28% and 15.92%, respectively.

Come here the CO concentration distribution in the same section is analyzed, and the simulation results are shown in Fig. 12. Although the removal rate of CO is zero, the air cleaning street lamps disperse the high concentration of CO sucked from the bottom of the street canyon to the top space by the outlets, which reduces CO concentration of breathing zones in the lower space in some cases. From Fig. 12, it can be seen that the purification effect of Design B is the best under the three wind directions. Design B has four air outlets and the CO concentration assigned to each outlet will be reduced. Therefore, the air reaching the pedestrian areas contains relatively little CO. For $\theta = 90^{\circ}$ Designs A, B, C and D make the mean CO concentration of breathing zone A decrease by 4.86%, 9.49%, 1.92% and 1.00%, respectively, and make the mean CO concentration of breathing zone B decrease by 6.11%, 3.89%, −2.98% and −1.38%, respectively; For $\theta = 45^{\circ}$ Designs A, B, C and D make the mean CO concentration of breathing zone A decrease by 3.33%, 3.84%, 2.76% and 2.53%, respectively, and make the mean CO concentration of breathing zone B decrease by 2.77%, 1.83%, −0.11% and −0.02%, respectively; For $\theta = 0^{\circ}$ Designs A, B, C and D make the mean CO concentration of breathing zones A and B decrease by 10.40%, 14.05%, 0.91% and 1.59% respectively.

The breathing zone A is the area where pollutants are easily concentrated. The reduction rates of PM, NO_x and CO in the breathing zone A are summarized in Table 3. Due to the different approaching wind direction and different removal efficiency for PM, NO_x and CO, the efficacy of air cleaning lamps is different. From Table 3, Design B achieves the highest frequency of optimal efficiency (highlighted by the underline in Table 3) in the listed scenarios. Therefore, the present study suggests that Design B has four 45° downward air outlets should be adopted. Further comparison is made for this design. Fig. 13 compares the mean PM, NO_x and CO concentrations of breathing zones A and B under different wind speeds and directions, where the dashed lines show the pollutant level outside the street canyon. By comparing with the results without air cleaning lamps shown in Figs. 8 and 9, the most obvious difference is that in many cases the mean pollutant concentration is below the dotted line, which indicates that the air quality in the pedestrian breathing areas inside the street canyon is better than that outside the street canyon. Especially under force Beaufort 1 (0.90 $m \cdot s^{-1}$), the volumetric purification capacity of 0.432 $m^3 \cdot s^{-1}$ of each air cleaning street lamp brings apparent pollutants reduction of the breathing zones compared with conventional street lamps (see the pollutant reduction rates of Design B in Table 3).

4.4. Discussion of the two air control measures

Reducing automobile exhaust emissions is an effective measure to improve the air quality in cities, which directly reduce the amount of pollutants in the environment. However, this study points out that air cleaning street lamps can actively remove pollutants from the pedestrian area, which improves air quality of the breathing zone even when pollutants keep flowing into the street canyon. It is conceivable that better effect can be achieved if both emission reduction measures and air cleaning street lamps are adopted. For the street canyon with the conventional street lamps discussed in the Section 4.1, the mean PM, NO_x and CO concentrations of breathing zone are highest under force Beaufort 1 (0.90 $m \cdot s^{-1}$). After adopting emission reduction (from China 5 standard to China 6b standard) and air cleaning street lamps (design B), numerical simulations give following appreciable pollutant reduction results: for $\theta = 90^{\circ}$, 45° and 0°, the mean PM concentration of breathing zone A decreases by 14.38%, 7.68% and 17.78%, respectively; the mean NO_x concentration of breathing zone A decreases by 24.92%, 21.33% and 29.03%, respectively; the mean CO concentration of breathing zone A decreases by 12.77%, 7.45% and 15.05%, respectively; the mean PM concentration of breathing zone B decreases by 5.47%, 2.52% and 17.78%, respectively; the mean NO_x concentration of breathing zone B decreases by 10.23%, 3.96% and 29.03%, respectively; the mean CO concentration of breathing zone B decreases by 4.61%,2.07% and 15.05%, respectively. Fig. 14 compares the purification rate of PM, NO_x and CO in breathing zone A by adopting emission reduction and air cleaning street lamps with the form of Design B, and simultaneously implementing the two measures under different wind speeds and winds directions. It can be found that the best way to improve the air quality in the street canyon is to combine emission reduction measures and air cleaning street lamps. It is also worth noting that in most of the cases studied, the effect of air cleaning street lamps is better than that of emission reduction. The air cleaning street lamp studied in this paper has relatively low cost, flexible operation, and can achieve better purification effect. Therefore, we believe that the air cleaning street lamp studied in this paper has a promising application for pollution reduction of city streets.

Table 3
Reduction rates of PM, NO_x and CO in the breathing zone A by different air cleaning street lamps under force Beaufort 1 (0.90 m s^{-1}) under different wind directions.

Design	PM			NO_x			CO		
	$\theta = 90^{\circ}$	$\theta = 45^{\circ}$	$\theta = 0^{\circ}$	$\theta = 90^{\circ}$	$\theta = 45^{\circ}$	$\theta = 0^{\circ}$	$\theta = 90^{\circ}$	$\theta = 45^{\circ}$	$\theta = 0^{\circ}$
A	5.96%	4.10%	13.27%	4.67%	3.81%	22.68%	4.86%	3.33%	10.40%
B	11.68%	4.62%	16.95%	11.29%	6.59%	24.20%	9.49%	3.84%	14.05%
C	13.73%	13.12%	12.20%	16.92%	19.22%	12.28%	1.92%	2.76%	0.91%
D	14.61%	14.19%	12.27%	13.78%	18.89%	15.92%	1.00%	2.53%	1.59%

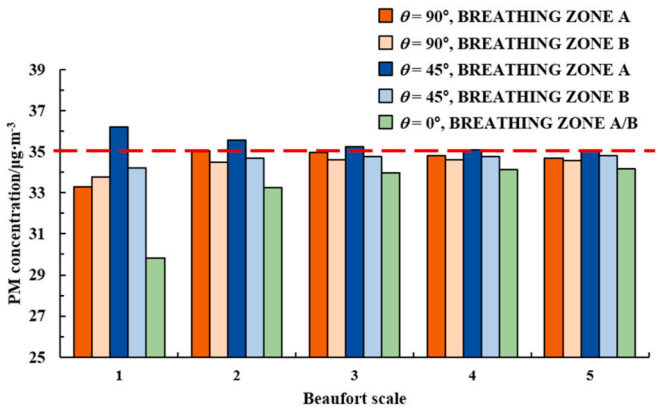

(a) Mean PM concentration

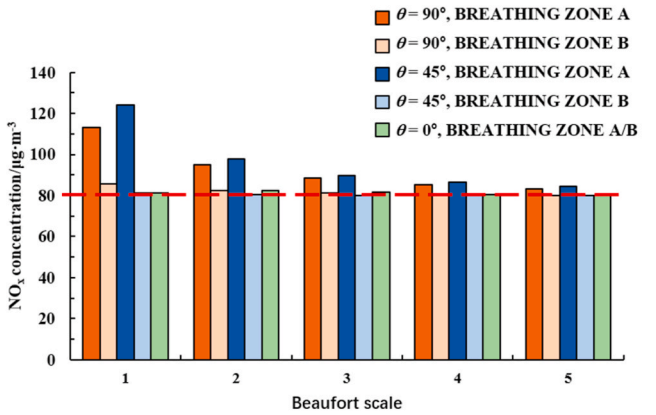

(b) Mean NO_x concentration

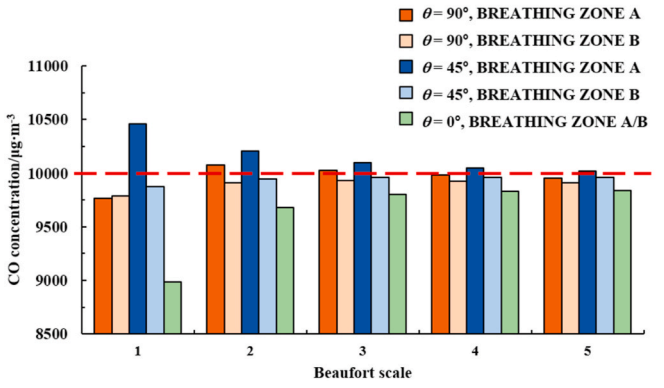

(c) Mean CO concentration

Fig. 13. Mean concentrations of three pollutants in breathing zones A and B under different wind directions and speeds (Design B).

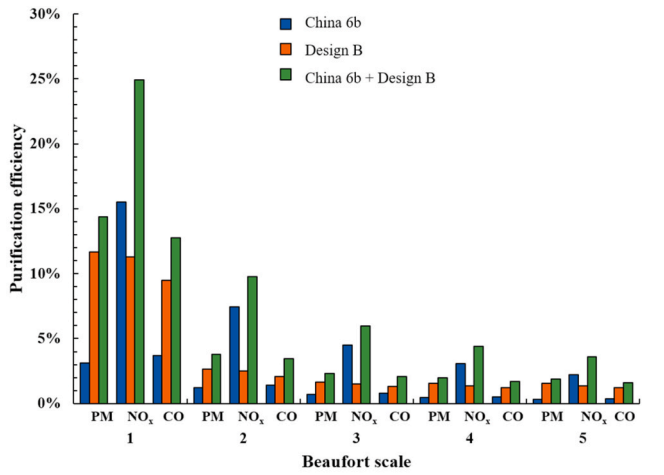

(a) $\theta = 90°$

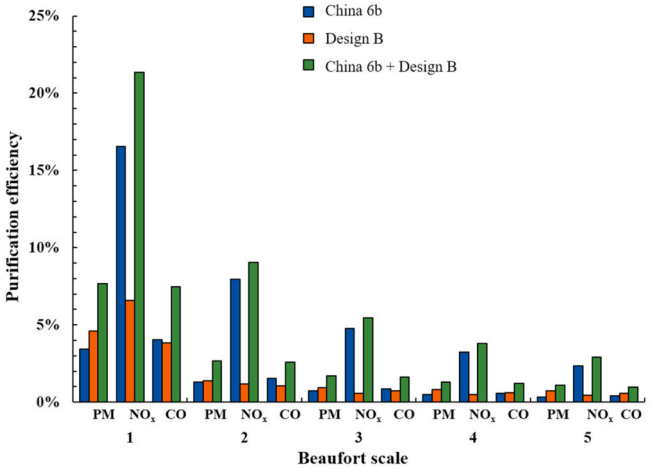

(b) $\theta = 45°$

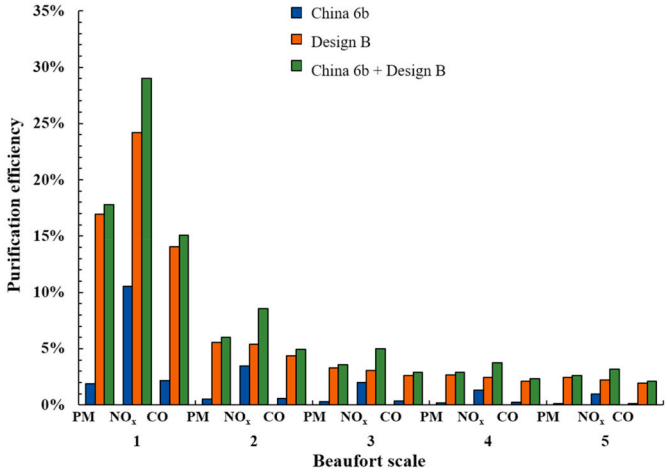

(c) $\theta = 0°$

Fig. 14. The purification efficiency of the breathing A under different measures.

5. Limitations and further study

Several limitations of the present study should be addressed. First, this work is carried out based on a steady RANS approach which is less accurate than Large Eddy Simulation (LES). Often the turbulent flow in the street canyon is affected by time-dependent inflow disturbance. Therefore, future work may adopt LES approach with time-dependent inflow conditions. Second, the simulations on street canyons with the air cleaning street lamps are lack of validation. Therefore, experiments on the air cleaning street lamps should be carried out in the future. Last, an ideal street canyon is studied in the present study. In the future study more urban configurations (such as street trees, vehicles) should be included.

6. Summary and conclusions

This paper provides a new idea to alleviate the air pollution in the street canyon, and puts forward the air cleaning street lamp to "actively" remove the air pollution inside the street canyon. Under three wind directions and five wind speeds, street canyons without street lamps, with conventional street lamps, and with four different air cleaning street lamps were simulated. The distributions of PM, NO_x and CO in the street canyon were studied. The effects of reducing emission, air cleaning street lamps and simultaneously implementing the two measures on reducing air pollution in the breathing zones inside the street canyon were compared. The main conclusions are as follows:

(1) The wind direction and wind speed have great influence on the pollutant dispersion in the street canyon. For the street canyon with street lamps without air cleaning function, the breathing zone A is heavily polluted, and the pollutant concentrations are the lowest under the parallel approaching wind direction. With the increase of wind speed, the pollutant concentrations decrease further, close to but still higher than those outside the street canyon.
(2) Adopting the emission reduction measure, from China 5 to China 6b, the pollutant concentrations of breathing zones decrease appreciably at lower wind velocity.
(3) Comparing four air outlet designs of the air cleaning street lamp, the lamp with four 45° downward air outlets is recommended due to the better effect. In most cases, the pollutant concentrations in the breathing zones inside the street canyon are lower than those outside the street canyon.
(4) In most of the cases, air cleaning street lamps are more effective for improving air quality in the breathing zones than reducing emissions from automobiles. A better way to improve the air quality in the street canyon is to combine both emission reduction measures and air cleaning street lamps. Under force Beaufort 1 ($0.90\ m{\cdot}s^{-1}$), simultaneously implementing the two measures, for $\theta = 90°$, 45° and 0°, the mean PM concentration of breathing zone A decreases by 14.38%, 7.68% and 17.78%, respectively; the mean NO_x concentration of breathing zone A decreases by 24.92%, 21.33% and 29.03%, respectively; the mean CO concentration of breathing zone A decreases by 12.77%, 7.45% and 15.05%, respectively; the mean PM concentration of breathing zone B decreases by 5.47%, 2.52% and 17.78%, respectively; the mean NO_x concentration of breathing zone B decreases by 10.23%, 3.96% and 29.03%, respectively; the mean CO concentration of breathing zone B decreases by 4.61%,2.07% and 15.05%, respectively.

Declaration of competing interest

The authors declare that they have no known competing financial interests or personal relationships that could have appeared to influence the work reported in this paper.

Acknowledgements

The authors would like to acknowledge the support provided by Key Project of National Natural Science Foundation of China "Multiscale simulation and measurement techniques of PEMFC stack used for vehicles" (51836005), the Foundation for Innovative Research Groups of the National Natural Science Foundation of China (No.51721004) and the 111 Project (B16038).

Appendix A. Supplementary data

Supplementary data to this article can be found online at https://doi.org/10.1016/j.buildenv.2021.107651.

References

[1] Health Effects Institute (HEI), Traffic-related Air Pollution: a Critical Review of the Literature on Emissions, Exposure, and Health Effects, Health Eff. Inst., Boston MA USA, 2010.
[2] H. Chen, M.S. Goldberg, P.J. Villeneuve, A systematic review of the relation between long-term exposure to ambient air pollution and chronic diseases, Rev. Environ. Health 23 (4) (2008) 243–298.
[3] R.D. Brook, S. Rajagopalan, C.A. Pope, et al., Particulate matter air pollution and cardiovascular disease: an update to the scientific statement from the American Heart Association, Circulation 121 (21) (2010) 2331–2378.
[4] K. Zhang, S. Batterman, Air pollution and health risks due to vehicle traffic, Sci. Total Environ. 450–451 (apr.15) (2013) 307–316.
[5] F. Laden, J. Schwartz, F.E. Speizer, D.W. Dockery, Reduction in fine particulate air pollution and mortality, Am. J. Respir. Crit. Care Med. 173 (6) (2006) 667–672.
[6] S.M. Salim, R. Buccolieri, A. Chan, S.D. Sabatino, Numerical simulation of atmospheric pollutant dispersion in an urban street canyon: comparison between RANS and LES, J. Wind Eng. Ind. Aerod. 99 (2–3) (2011) 103–113.
[7] R. Britter, M. Schatzmann, Background and justification document to support the model evaluation guidance and protocol, COST Action 732 (2007).
[8] R.E. Britter, S.R. Hanna, Flow and dispersion in urban areas, Annu. Rev. Fluid Mech. 35 (1) (2003) 469–496.
[9] S. Vardoulakis, B.-E.A. Fisher, K. Pericleous, F.-N. Gonzalez, Modelling air quality in street canyons: a review, Atmos. Environ. 37 (2) (2003) 155–182.
[10] K. Ahmad, M. Khare, K.K. Chaudhry, Wind tunnel simulation studies on dispersion at urban street canyons and intersections - a review, J. Wind Eng. Ind. Aerod. 93 (9) (2005) 697–717.
[11] B. Blocken, T. Stathopoulos, J.P.A.J. Van Beeck, Pedestrian-level wind conditions around buildings: review of wind-tunnel and CFD techniques and their accuracy for wind comfort assessment, Build. Environ. 100 (5) (2016) 50–81.
[12] C. Wang, Q. Li, Z.H. Wang, Quantifying the impact of urban trees on passive pollutant dispersion using a coupled large-eddy simulation–Lagrangian stochastic model, Build. Environ. 145 (NOV) (2018) 33–49.
[13] C. Gromke, B. Blocken, Influence of avenue-trees on air quality at the urban neighborhood scale. Part II: traffic pollutant concentrations at pedestrian level, Environ. Pollut. 196 (2015) 176–184.
[14] X. Li, C. Liu, D. Leung, K.M. Leung, K.M. Lam, Recent progress in CFD modelling of wind field and pollutant transport in street canyons, Atmos. Environ. 40 (29) (2006) 5640–5658.
[15] D.C. Smith, Later model year light-duty vehicle greenhouse gas emissions and corporate average fuel economy standards, Fed. Regist. 62 (4) (2017) 568–569, 2012.
[16] G. Fontaras, P. Dilara, The evolution of European passenger car characteristics 2000–2010 and its effects on real-world CO_2 emissions and CO_2 reduction policy, Energy Pol. 49 (202) (2012) 719–730.
[17] Y. Wu, S. Zhang, J. Hao, et al., On-road vehicle emissions and their control in China: a review and outlook, Sci. Total Environ. 574 (JAN.1) (2017) 332–349.
[18] J. Gallagher, R. Baldauf, C.H. Fuller, P. Kumar, W.G. Laurence, M. Aonghus, Passive methods for improving air quality in the built environment: a review of porous and solid barriers, Atmos. Environ. 120 (NOV) (2015) 61–70.
[19] K.V. Abhijith, P. Kumar, J. Gallagher, A. McNabola, R. Baldauf, F. Pilla, B. Pulvirenti, Air pollution abatement performances of green infrastructure in open road and built-up street canyon environments - a review, Atmos. Environ. 162 (Aug) (2017) 71–86.
[20] J.T. Steffens, D.K. Heist, S.G. Perry, K.M. Zhang, Modeling the effects of a solid barrier on pollutant dispersion under various atmospheric stability conditions, Atmos. Environ. 69 (APR) (2013) 76–85.
[21] J. Gallagher, L. Gill, A. Mcnabola, The passive control of air pollution exposure in Dublin, Ireland: a combined measurement and modelling case study, Sci. Total Environ. 458–460 (aug. 1) (2013) 331–343.
[22] K.V. Abhijith, S. Gokhale, Passive control potentials of trees and on-street parked cars in reduction of air pollution exposure in urban street canyons, Environ. Pollut. 204 (september) (2015) 99–108.
[23] A. Mcnabola, New Directions: passive control of personal air pollution exposure from traffic emissions in urban street canyons, Atmos. Environ. 44 (24) (2010) 2940–2941.
[24] Codasc, Concentration Data of Street Canyons. Internet Database, Karlsruhe Institute of Technology KIT, Germany, 2008. www.codasc.de [WWW Document].
[25] C. Gromke, R. Buccolieri, S-Di Sabatino, B. Ruck, Dispersion study in a street canyon with tree planting by means of wind tunnel and numerical investigations – evaluation of CFD data with experimental data, Atmos. Environ. 42 (37) (2008) 8640–8650.
[26] Y. Huang, P.G. Wang, Z.Y. Wang, et al., Protonated g-C_3N_4/Ti^{3+} self-doped TiO_2 nanocomposite films: room-temperature preparation, hydrophilicity, and application for photocatalytic NO_x removal, Appl. Catal. B Environ. 240 (2018) 122–131.
[27] Y. Huang, Personal Communication, 2019.
[28] S.M. Salim, S.C. Cheah, A. Chan, Numerical simulation of dispersion in urban street canyons with avenue-like tree plantings: comparison between RANS and LES, Build. Environ. 46 (9) (2011) 1735–1746.
[29] A.P.R. Jeanjean, G. Hinchliffe, W.A. Mcmullan, et al., A CFD study on the effectiveness of trees to disperse road traffic emissions at a city scale, Atmos. Environ. 120 (2015) 1–14.
[30] W.Q. Tao, Numerical Heat Transfer, second ed., Xi'an Jiaotong University Press, Xi'an, China, 2001.
[31] ANSYS, ANSYS FLUENT 14, 0 Theory Guide, ANSYS, Inc., 2014.

[32] S. Vranckx, P. Vos, B. Maiheu, S. Janssen, Impact of trees on pollutant dispersion in street canyons: a numerical study of the annual average effects in Antwerp, Belgium, Sci. Total Environ. 532 (nov.1) (2015) 474–483.
[33] F. Xue, X. Li, The impact of roadside trees on traffic released PM10 in urban street canyon: aerodynamic and deposition effects, Sustainable Cities & Society 30 (2017) 195–204.
[34] Y. Tominaga, T. Stathopoulos, CFD modeling of pollution dispersion in building array: evaluation of turbulent scalar flux modeling in RANS model using LES results, J. Wind Eng. Ind. Aerod. 104–106 (none) (2012) 484–491.
[35] Yang Xing, Peter Brimblecombe, Dispersion of traffic derived air pollutants into urban parks, Sci. Total Environ. 622–623 (2018) 576–583.
[36] S. Holmberg, Y. Li, Modelling of the indoor environment-particle dispersion and deposition, Indoor Air 8 (1998) 113–122.
[37] B. Zhao, Z. Zhang, X. Li, Numerical study of the transport of droplets or particles generated by respiratory system indoors, Build. Environ. 40 (8) (2005) 1032–1039.
[38] C. Gromke, B. Blocken, Influence of avenue-trees on air quality at the urban neighborhood scale. Part I: quality assurance studies and turbulent Schmidt number analysis for RANS CFD simulations, Environ. Pollut. 196 (2015) 214–223.
[39] Y. Yuan, K. Yang, C. Du, X. Fu, Study on Schmidt number of pollutant diffusion in urban street atmosphere, Procedia Engineering 205 (2017) 1711–1717.
[40] W.C. Hinds, Aerosol Technology: Properties, Behavior, and Measurement of Airborne Particles, Wiley, New York, 1999.
[41] J. Franke, A. Hellsten, H. Schlünzen, et al., Best Practice Guideline for the CFD Simulation of Flows in the Urban Environment, COST Office, Brussels, 2007, pp. 1–33.
[42] P.J. Richards, R.P. Hoxey, Appropriate boundary conditions for computational wind engineering models using the k- turbulence model, J. Wind Eng. Ind. Aerod. 46–47 (1993) 145–153.
[43] B. Blocken, T. Stathopoulos, J. Carmeliet, CFD simulation of the atmospheric boundary layer: wall function problems, Atmos. Environ. 41 (2) (2007) 238–252.
[44] K. Ahmad, M. Khare, K.K. Chaudhry, Wind tunnel simulation studies on dispersion at urban street canyons and intersections - a review, J. Wind Eng. Ind. Aerod. 93 (9) (2005) 697–717.
[45] J.C. Zavala-Reyes, A.P.R. Jeanjean, R.J. Leigh, et al., Studying human exposure to vehicular emissions using computational fluid dynamics and an urban mobility simulator: the effect of sidewalk residence time, vehicular technologies and a traffic-calming device, Sci. Total Environ. 687 (OCT.15) (2019) 720–731.
[46] J.C. Chang, S.R. Hanna, Air quality model performance evaluation, Meteorol. Atmos. Phys. 87 (1–3) (2004) 167–196.
[47] S. Hanna, J. Chang, Acceptance criteria for urban dispersion model evaluation, Meteorol. Atmos. Phys. 116 (3–4) (2012) 133–146.
[48] R. Buccolieri, S.M. Salim, L.S. Leo, et al., Analysis of local scale tree–atmosphere interaction on pollutant concentration in idealized street canyons and application to a real urban junction, Atmos. Environ. 45 (9) (2011) 1702–1713.